Article

Cell

Histone H3 Threonine Phosphorylation Regulates Asymmetric Histone Inheritance in the *Drosophila* Male Germline

Graphical Abstract

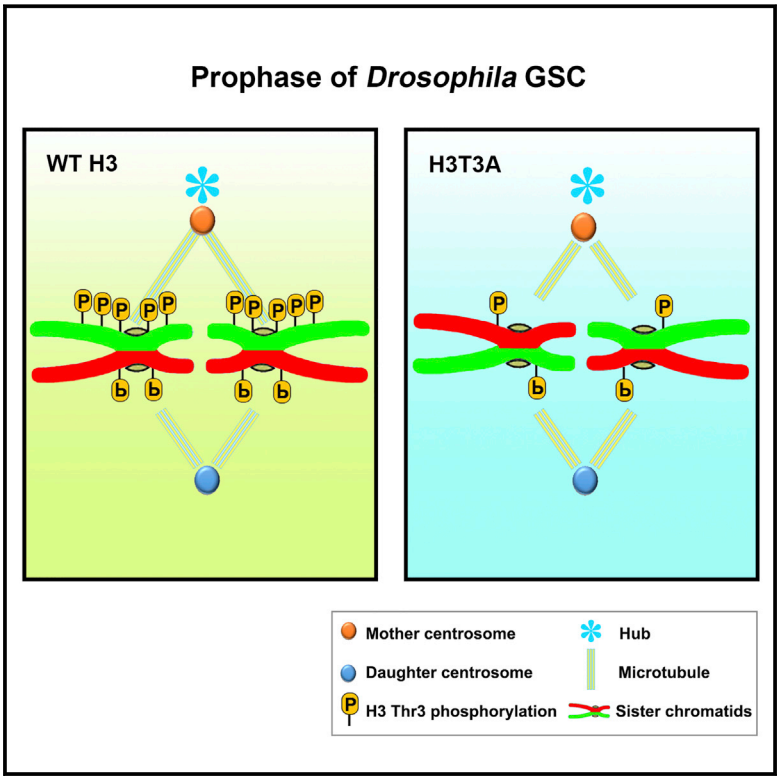

Highlights

- Pre-existing versus newly synthesized H3 are separable in prophase germline stem cell
- H3 threonine 3 phosphorylation distinguishes pre-existing from newly synthesized H3
- Both H3T3A and H3T3D mutations randomize H3 inheritance patterns
- Reducing H3T3 kinase Haspin enhances the H3T3A but suppresses the H3T3D phenotypes

Authors

Jing Xie, Matthew Wooten, Vuong Tran, ..., Christine Simbolon, Eric Betzig, Xin Chen

Correspondence

xchen32@jhu.edu

In Brief

A transient mitosis-specific phosphate modification on histone H3 distinguishes pre-existing and newly synthesized histones and is required for the asymmetric segregation of sister chromatids—one enriched with new histones and the other with old—during stem cell division.

Xie et al., 2015, Cell *163*, 920–933
November 5, 2015
http://dx.doi.org/10.1016/j.cell.2015.10.002

CellPress

Cell

Article

Histone H3 Threonine Phosphorylation Regulates Asymmetric Histone Inheritance in the *Drosophila* Male Germline

Jing Xie,[1] Matthew Wooten,[1] Vuong Tran,[1,3] Bi-Chang Chen,[2,4] Caitlin Pozmanter,[1] Christine Simbolon,[1] Eric Betzig,[2] and Xin Chen[1,*]

[1]Department of Biology, Johns Hopkins University, Baltimore, MD 21218, USA
[2]HHMI, Janelia Research Campus, 19700 Helix Drive, Ashburn, VA 20147, USA
[3]Present address: Fred Hutchinson Cancer Research Center, 1100 Fairview Avenue North Seattle, Seattle, WA 98109, USA
[4]Present address: Research Center for Applied Science, Academia Sinica, Taipei, 11529, Taiwan
*Correspondence: xchen32@jhu.edu
http://dx.doi.org/10.1016/j.cell.2015.10.002

SUMMARY

A long-standing question concerns how stem cells maintain their identity through multiple divisions. Previously, we reported that pre-existing and newly synthesized histone H3 are asymmetrically distributed during *Drosophila* male germline stem cell (GSC) asymmetric division. Here, we show that phosphorylation at threonine 3 of H3 (H3T3P) distinguishes pre-existing versus newly synthesized H3. Converting T3 to the unphosphorylatable residue alanine (H3T3A) or to the phosphomimetic aspartate (H3T3D) disrupts asymmetric H3 inheritance. Expression of H3T3A or H3T3D specifically in early-stage germline also leads to cellular defects, including GSC loss and germline tumors. Finally, compromising the activity of the H3T3 kinase Haspin enhances the H3T3A but suppresses the H3T3D phenotypes. These studies demonstrate that H3T3P distinguishes sister chromatids enriched with distinct pools of H3 in order to coordinate asymmetric segregation of "old" H3 into GSCs and that tight regulation of H3T3 phosphorylation is required for male germline activity.

INTRODUCTION

Epigenetic phenomena are heritable changes in gene expression or function that can persist throughout many cell divisions without alterations in primary DNA sequences. By regulating differential gene expression, epigenetic processes are able to direct cells with identical genomes to become distinct cell types in humans and other multicellular organisms. However, with the exception of DNA methylation, little is known about the molecular pathways leading to epigenetic inheritance (Bonasio et al., 2010; Martin and Zhang, 2007).

Prior research has shown that epigenetic events play particularly important roles in ensuring both proper maintenance and differentiation of several stem cell populations. Many types of adult stem cells undergo asymmetric cell division to generate a self-renewed stem cell and a daughter cell that will subsequently differentiate (Betschinger and Knoblich, 2004; Clevers, 2005; Inaba and Yamashita, 2012; Morrison and Kimble, 2006). Misregulation of this balance leads to many human diseases, ranging from cancer to tissue dystrophy to infertility. However, the mechanisms of stem cell epigenetic memory maintenance as well as how loss of this memory contributes to disease remain unknown.

Recently, we found that during the asymmetric division of the *Drosophila* male germline stem cell (GSC), the pre-existing histone 3 (H3) is selectively segregated to the self-renewed GSC daughter cell whereas newly synthesized H3 is enriched in the differentiating daughter cell known as a gonialblast (GB) (Tran et al., 2012) (Figure 1A). In contrast, the histone variant H3.3, which is incorporated in a replication-independent manner, does not exhibit such an asymmetric pattern. Furthermore, we found that asymmetric H3 inheritance occurs specifically in asymmetrically dividing GSCs, but not in the symmetrically dividing progenitor cells. These findings demonstrate that global asymmetric H3 histone inheritance possesses both molecular and cellular specificity. We proposed the following model to explain our findings.

First, the cellular specificity exhibited by the H3 histone suggests that global asymmetric histone inheritance occurs uniquely in a cell-type (GSC) where the mother cell must divide to produce two daughter cells each with a unique cell fate. Because this asymmetry is not observed in symmetrically dividing GB cells, we propose asymmetric histone inheritance to be a phenomenon specifically employed by GSCs to establish unique epigenetic identities in each of the two daughter cells. Second, as stated previously, a major difference between H3 and H3.3 is that H3 is incorporated to chromatin during DNA replication, while H3.3 variant is incorporated in a replication-independent manner. Because this asymmetric inheritance mode is specific to H3, we propose a two-step model to explain asymmetric H3 inheritance: (1) prior to mitosis, pre-existing and newly synthesized H3 are differentially distributed on the two sets of sister chromatids, and (2) during mitosis, the set of sister chromatids containing pre-existing H3 is segregated to GSCs, while the set of sister chromatids enriched with newly synthesized H3

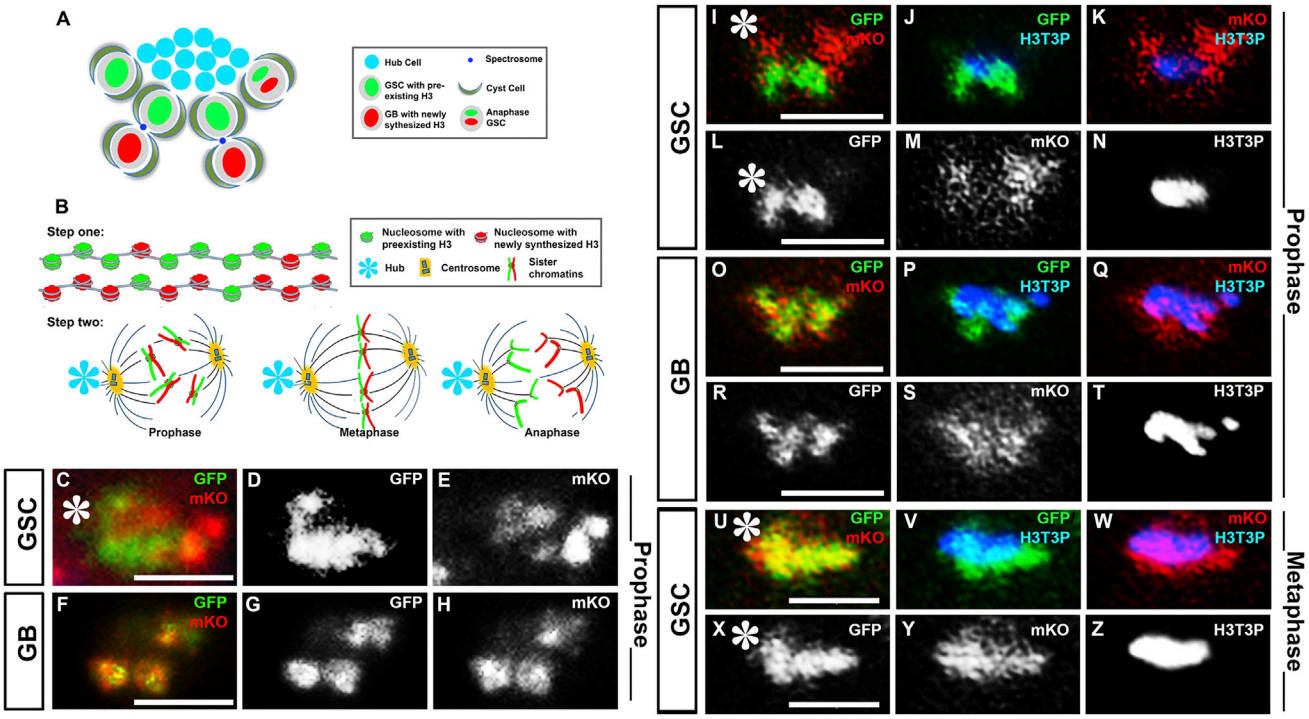

Figure 1. H3T3P Distinguishes Pre-existing H3-GFP from Newly Synthesized H3-mKO in Mitotic Male GSCs

(A) A visual representation of the *Drosophila* testis tip showing the asymmetric H3 inheritance during male GSC asymmetric cell division.

(B) A schematic diagram of a two-step model to explain how the asymmetric epigenome is established during S-phase (step one) and recognized followed by asymmetric segregation in M-phase (step two) GSC, adapted from Tran et al. (2013).

(C–E) A prophase GSC where GFP and mKO signals are separable.

(F–H) A prophase GB where GFP and mKO signals are overlapping.

(I–N) A prophase GSC where GFP and mKO signals are separable at some chromosomal region (I, L, and M). Immunostaining using anti-H3T3P (N) showed H3T3P co-localization more with GFP (J, L, and N) than with mKO (K, M, and N).

(O–T) A prophase GB where GFP and mKO signals are overlapping (O, R, and S) and no preference of H3T3P (T) with either GFP (P and R) or mKO (Q and S).

(U–Z) A metaphase GSC where GFP and mKO signals are indistinguishable (U, X, and Y), H3T3P (Z) overlaps with both GFP (V and X) and mKO (W and Y).

Asterisks in (C), (I), (L), (U), and (X), hub. Scale bars, 5 μm.

See also Figure S1.

is segregated to the GB that differentiates (Tran et al., 2012, 2013) (Figure 1B).

RESULTS

H3T3P Distinguishes Pre-existing H3 and Newly Synthesized H3 in Mitotic Male GSCs

To test our proposed two-step model, we used a temporally controlled dual-color system to precisely label pre-existing H3 with GFP and newly synthesized H3 with monomeric Kusabira-Orange (mKO) (Tran et al., 2012). Asymmetric segregation of H3-GFP and H3-mKO was clearly visualized in anaphase and telophase GSCs imaged during the second mitosis following heat-shock-induced switch from *H3-GFP*- to *H3-mKO*-coding sequence (Tran et al., 2012). Here, we show that H3-GFP and H3-mKO signals are already separable at some chromosomal region in prophase GSCs (Figures 1C–1E), likely in regions with less tight cohesion between sister chromatids. Such a separation was not detected in a control prophase GB (Figures 1F–1H). These results are consistent with the hypothesis that the differential distribution between pre-existing H3-GFP and newly synthesized H3-mKO is established prior to mitosis in GSCs (Figure 1B, step one). By contrast, such a separation was not detected using a H3.3 dual-color transgene under the same heat-shock regime (Figure S1A), consistent with our previous report that H3.3 is inherited symmetrically (Tran et al., 2012).

When immunostaining experiments were performed using an antibody recognizing a mitosis-enriched phosphorylation at threonine 3 of H3 (H3T3P) (Dai et al., 2005; Polioudaki et al., 2004), the H3T3P signal (Figures 1J, 1K, and 1N) showed more co-localization with H3-GFP (Figures 1I and 1L) than with H3-mKO (Figures 1I and 1M) in prophase GSCs where separation between H3-GFP and H3-mKO could be visualized (Figures 1I, 1L, and 1M). By contrast, H3-GFP signals and H3-mKO signals were not separable in prophase GBs, (Figures 1O, 1R, and 1S) and H3T3P did not distinguish between them (Figures 1P, 1Q, and 1T). Furthermore, when sister chromatids congressed to the equator in metaphase GSCs, such a distinction became undetectable (Figures 1U–1Z), suggesting that H3T3P distinguishes sister chromatids enriched with pre-existing H3 from those enriched with newly synthesized H3 in prophase GSCs.

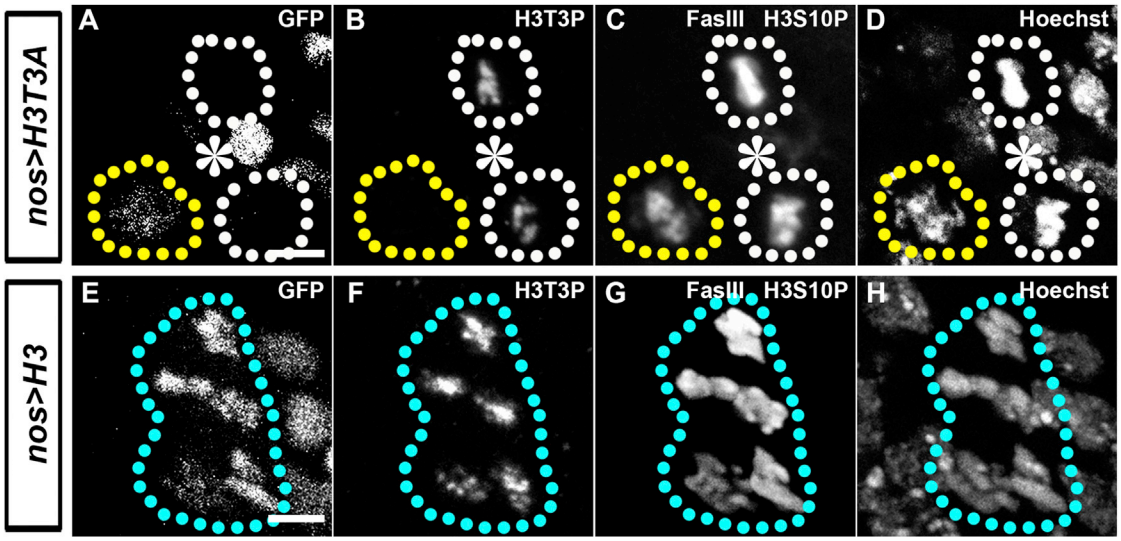

Figure 2. Expression of an H3T3A Transgene Greatly Reduces H3T3P in Mitotic Germ Cells

(A–D) Tip of a testis expressing *nos>H3T3A-GFP* stained with antibodies against a hub marker FasIII, H3T3P, and H3S10P. A prophase germ cell (yellow dotted outline) expressing H3T3A-GFP (A) is lack of H3T3P (B) but has abundant H3S10P (C) that co-localizes with condensed chromosome labeled by Hoechst staining (D). Two mitotic CySCs (white dotted outline) without H3T3A-GFP (A) has both H3T3P (B) and H3S10P (C) signals co-localized with condensed chromosome labeled by Hoechst staining (D). Asterisks, hub.

(E–H) Mitotic germ cells (cyan dotted outline) expressing *nos>H3-GFP* (E) as a control have both H3T3P (F) and H3S10P (G) signals co-localized with condensed chromosome labeled by Hoechst staining (H). Scale bars, 5 μm.

See also Figure S2.

Consistent with this potential function of H3T3P, immunostaining signals of H3T3P were only detectable in prophase (Figures 1N and S1D) to metaphase (Figures 1Z, and S1D), but not in late anaphase (Figure S1D) GSCs. By contrast, immunostaining using an antibody against another mitosis-enriched H3S10P (phosphorylation at serine 10 of H3) showed abundant signal throughout mitosis (Figure S1D). Furthermore, the signal from H3T3P immunostaining (Figure S1E) was enriched, but not restricted, to the centromeric region labeled with an antibody against a centromere-specific H3 variant centromere identifier (Cid) (Figure S1E). In summary, the temporal and spatial distributions of H3T3P in *Drosophila* male germ cells are comparable to what has been reported in other cell types from other systems (Caperta et al., 2008; Dai et al., 2005; Escribá and Goday, 2013; Markaki et al., 2009; Wang et al., 2010).

Expression of an H3T3A Transgene Greatly Reduces H3T3P in Mitotic Germ Cells

To understand the function of H3T3P in male germ cells, we generated fly lines with an H3-GFP transgene carrying a point mutation that converts T3 to the unphosphorylatable alanine (Ala or A, H3T3A). Expression of the H3T3A-GFP transgene in early germ cells by the *nanos-Gal4* (*nos-Gal4*) driver (Van Doren et al., 1998) greatly reduced the H3T3P signal (yellow versus white outlined cells in Figures 2A and 2B). This reduction of immunostaining signal was specific to H3T3P, as immunostaining using anti-H3S10P showed normal signals in H3T3A-expressing cells (yellow versus white outlined cells in Figure 2C). As a control, expression of the wild-type H3-GFP had no effect on either H3T3P (Figures 2E and 2F) or H3S10P (Figure 2G) signals.

Because endogenous H3 is still abundant in testes in which early germ cells are enriched with *nos*-driving H3T3A expression (Figures S2A and S2B), the absence of H3T3P signal suggests a dominant negative effect of H3T3A. The dominant negative effect of point mutations of H3 has recently been observed with several residues of histone H3 (Herz et al., 2014; Lewis et al., 2013).

Expression of H3T3A Changes the Asymmetric H3 Segregation Pattern in Mitotic GSCs

Because expression of the H3T3A provides a loss-of-function condition for H3T3P (Figures 2, S2C, and S2D), we next explored whether asymmetric histone segregation is affected in H3T3A-expressing GSCs using the dual-color labeling strategy (Figure 3A). As a control, we used a similar system with wild-type H3 and found that pre-existing H3-GFP and newly synthesized H3-mKO are asymmetrically segregated in telophase GSCs during the second mitosis after heat-shock-induced genetic switch (Figures 3B–3D), consistent with our previous report (Tran et al., 2012). By contrast, we found a dramatic shift in histone inheritance patterns from predominantly asymmetric to predominantly symmetric pattern (Figures 3H–3J), using the dual-color transgene with H3T3A (Figure 3A). Although the majority of GSCs expressing H3T3A exhibited a symmetric pattern of histone inheritance (Figures 3H–3J), we could still detect the conventional asymmetric pattern resembling that of wild-type H3 in telophase GSCs (Figures 3E–3G). Surprisingly, we also observed the inverted asymmetric pattern (Figures 3K–3M).

We reason that if pre-existing and newly synthesized histones are randomly incorporated during the first step (Figure 1B), no separation between GFP and mKO signals should be detectable

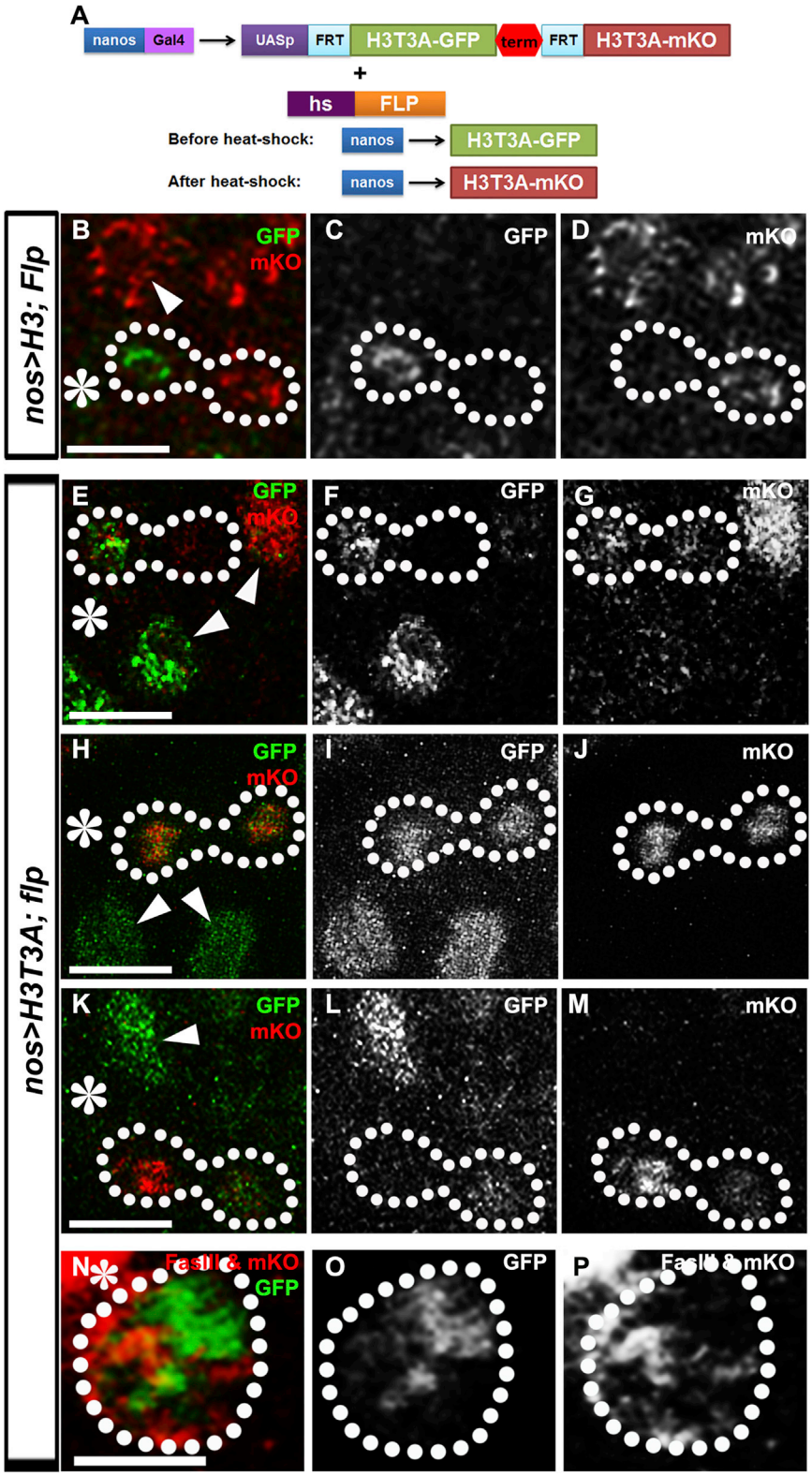

Figure 3. Expression of H3T3A Changes the Asymmetric H3 Segregation Pattern in Mitotic GSCs

(A) A schematic diagram showing the dual color-switch design that expresses pre-existing H3T3A-GFP and newly synthesized H3T3A-mKO by heat-shock treatment, as adapted from Tran et al. (2012).

(B–D) A telophase GSC expressing *nos>FRT-H3-GFP-PolyA-FRT-H3-mKO-PolyA* (*nos>H3*) during the second mitosis after heat-shock-induced genetic switch show conventional asymmetric segregation pattern.

(E–M) Telophase GSCs expressing *nos>FRT-H3T3A-GFP-PolyA-FRT-H3T3A-mKO-PolyA* (*nos>H3T3A*) during the second mitosis after heat-shock-induced genetic switch show conventional asymmetric segregation pattern (E–G), symmetric pattern (H–J), or inverted asymmetric pattern (K–M).

(N–P) A prophase GSC expressing *nos>FRT-H3T3A-GFP-PolyA-FRT-H3T3A-mKO-PolyA* (*nos>H3T3A*) during the second mitosis after heat-shock-induced genetic switch show separable GFP and mKO signals. Asterisk, hub; white dotted outline, mitotic GSCs at telophase (B–M) or prophase (N–P); arrowheads, interphase GSCs or GBs that show much less condensed nuclei. Scale bars, 5 μm.

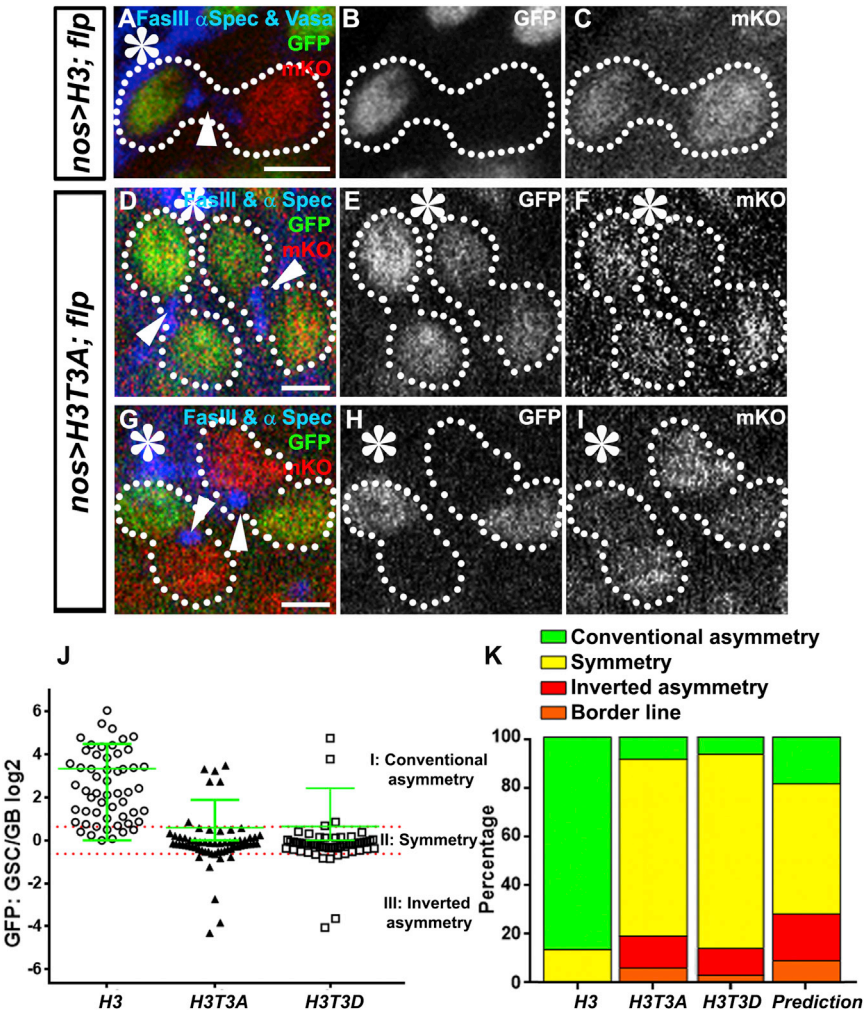

Figure 4. Expression of H3T3A or H3T3D Changes Pre-existing and Newly Synthesized H3 Distribution Patterns in Post-Mitotic GSC-GB Pairs

(A–I) Immunostaining signals using antibodies against a hub marker FasIII and spectrosome/fusome marker α-spectrin in testes from *nos>FRT-H3-GFP-PolyA-FRT-H3-mKO-PolyA* (*nos>H3*, A–C) or *nos>FRT-H3T3A-GFP-PolyA-FRT-H3T3A-mKO-PolyA* (*nos>H3T3A*, D–I) males after the second mitosis upon heat-shock-induced genetic switch. Asterisk, hub; white dotted outline, post-mitotic GSC-GB pairs; arrowheads, spectrosome structure in between GSC and GB cells. Scale bars, 5 μm.

(J) Quantification of the ratio of GFP (y axis: $\log_2$ scale) fluorescence intensity in GSC-GB pairs (see Figures S3A, S3B, and Table S1 for details): *nos>H3* (open circle, n = 55), *nos>H3T3A* (solid triangle, n = 64), and *nos>H3T3D* (open square, n = 57). Red dotted outline delineates symmetric distribution zone (see explanations below). H3 (n = 55): GSC/GB GFP ratio = 10.11 ± 1.66 ($p < 10^{-4}$ for the ratio >1, one-tailed t test). H3T3A (n = 64): GSC/GB GFP ratio = 1.50 ± 0.28 ($p > 0.05$ therefore is insignificantly different from 1, two-tailed t test). H3T3D (n = 57): GSC/GB GFP ratio = 1.56 ± 0.51 ($p > 0.05$ therefore is insignificantly different from 1, two-tailed t test). All ratios = Avg ± SE; p value, one sample t test.

(K) Percentage of GSC-GB pairs with conventional asymmetric (GFP in GSC/GB >1.55), symmetric (GSC/GB GFP ratio between 1–1.45 and GB/GSC GFP ratio between 1–1.45), inverted asymmetric (GFP in GB/GSC >1.55), and borderline (GSC/GB GFP ratio between 1.45–1.55 and GB/GSC GFP ratio between 1.45–1.55) patterns, respectively in *nos>H3*, *nos>H3T3A*, and *nos>H3T3D* testes, as well as the predicted patterns according to randomized segregation modeling (Table S2). In *nos>H3* testes, conventional asymmetric: 87.3% (48/55); symmetric: 12.7% (7/55); no inverted asymmetric or borderline pairs. In *nos>H3T3A* testes, conventional asymmetric: 9.4% (6/64); symmetric: 71.9% (46/64); inverted asymmetric: 12.5% (8/64); borderline: 6.3% (4/64). In *nos>H3T3D* testes, conventional asymmetric: 7.0% (4/57); symmetric: 79.0% (45/57); inverted asymmetric: 10.5% (6/57); borderline: 3.5% (2/57). Predicted patterns: conventional asymmetric: 18.7% (12/64); symmetric: 53.1% (34/64); inverted asymmetric: 18.7% (12/64); borderline: 9.4% (6/64). See also Figures S3A and S3B and Tables S1 and S2.

during GSC asymmetric division. The fact that we could still identify conventional and inverted asymmetric segregation patterns in telophase GSCs (Figures 3E–3G and 3K–3M) suggests that the establishment of histone asymmetry prior to mitosis may not be affected. The observed defects in proper asymmetric segregation therefore arise upon mitotic entry when sister chromatids containing different populations of H3 need to be recognized and segregated to the appropriate daughter cell (Figure 1B, step two). Consistent with this hypothesis, separable H3T3A-GFP and H3T3A-mKO could still be detected in prophase GSCs (Figures 3N–3P and S1B), but not in a control prophase GB (Figure S1C).

Expression of H3T3A Changes H3 Distribution Patterns in Post-Mitotic GSC-GB Pairs

Since mitotic GSCs account for <2% among all GSCs (Sheng and Matunis, 2011; Yadlapalli et al., 2011; Yadlapalli and Yamashita, 2013), we next examined post-mitotic GSC-GB pairs derived from GSC asymmetric divisions to quantify histone inheritance patterns (Tran et al., 2012) (Experimental Procedures).

In contrast to the conventional asymmetric distribution pattern in wild-type H3-expressing GSC-GB pair (Figures 4A–4C), we observed symmetric (Figures 4D–4F), conventional asymmetric (left pair in Figures 4G–4I), and inverted asymmetric (right pair in Figures 4G–4I) distribution patterns in post-mitotic GSC-GB pairs. These data are consistent with what we have observed with mitotic GSCs (Figures 3E–3M).

Next, we quantified the percentage of each of these distribution patterns. We mainly used GFP signal to account for different patterns, for example, in Figure 4J: the conventional asymmetric patterns are in zone I, with GFP ratio in GSC/GB >1.55; the symmetric patterns are in zone II, with GFP ratio in GSC/GB <1.45 but >0.69 (i.e., GB/GSC <1.45); and the inverted asymmetric patterns are in zone III, with GFP ratio in GB/GSC >1.55.

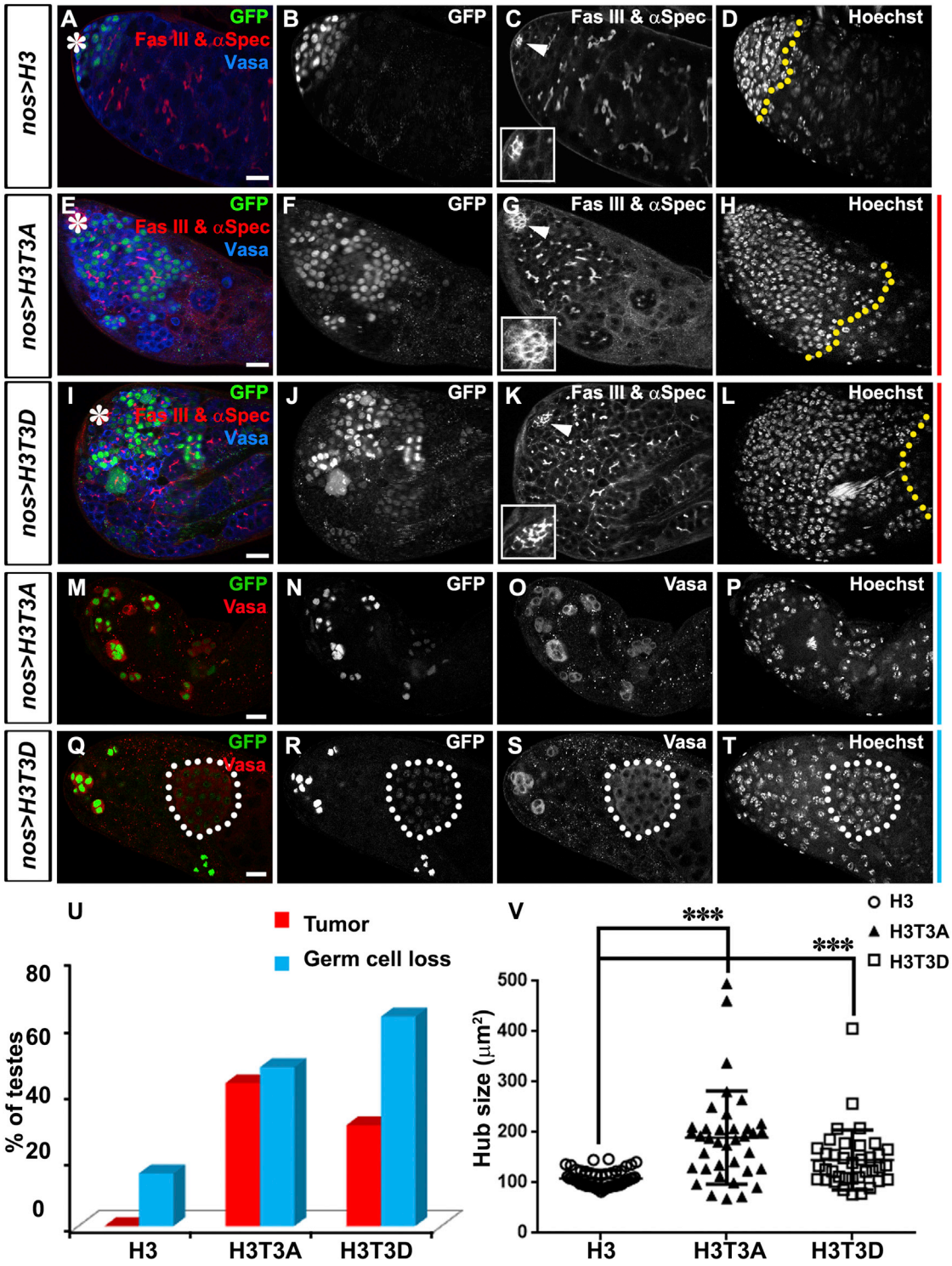

Figure 5. Both Germline and Somatic Gonadal Cells Show Defects in *nos>H3T3A* or *nos>H3T3D* Testes

(A–L) Immunostaining using antibodies against a hub marker FasIII and spectrosome/fusome marker α-spectrin in testes from *nos>H3-GFP* (A–D), *nos>H3T3A-GFP* (E–H), or *nos>H3T3D-GFP* (I–L) males 7 days after eclosion. Asterisks in (A), (E), and (I), hub; arrowheads in (C), (G), and (K) point to the hub region, which are shown with higher magnification in insets: hub size increases in *nos>H3T3A-GFP* (inset in G) or *nos>H3T3D-GFP* (inset in K) testes, but not in *nos>H3-GFP* (inset in C) testes. Early-stage germ cells, as determined by *nos*-driven GFP expression (B, F, and J), and nuclear morphology (Chen et al., 2013; Tran et al., 2000) are delineated by the yellow dotted lines in (D), (H), and (L). Scale bars, 20 μm.

(legend continued on next page)

The ~1.5-fold cutoff is based on the quantification range of symmetric H3 distribution in spermatogonial cells and symmetric H3.3 distribution in GSC-GB pairs (Tran et al., 2012, 2013). We reasoned that GFP ratio reflects the establishment of asymmetric histone distribution on sister chromatids more reliably than mKO ratio for two reasons. First, when we measured mKO fluorescence intensity in post-mitotic GSC-GB pairs, both cells are actively undergoing S phase for the next mitosis and exhibit robust incorporation of mKO-labeled newly synthesized histones (Figure 4C). Second, any histone turn-over that incorporates newly synthesized mKO-labeled histones (Deal et al., 2010; Dion et al., 2007) during processes such as transcription may not be sister chromatid-specific.

When we quantified the GFP distribution patterns in post-mitotic GSC-GB pairs in H3T3A-expressing testes (Figures 4J and S3A), we found that 71.9% (46/64) of pairs showed a symmetric pattern of inheritance (Figure 4K; Table S1). By contrast, in wild-type H3-expressing testes, 87.3% (48/55) of pairs showed an asymmetric pattern of inheritance (Figure 4K; Table S1). Moreover, in H3T3A-expressing testes, asymmetric patterns could be observed in two distinct modes at lower frequencies: 9.4% (6/64) conventional asymmetry, 12.5% (8/64) inverted asymmetry, and 6.3% (4/64) at the borderline (1.45- to 1.55-fold) between asymmetry and symmetry (Figure 4K; Table S1). Noticeably, no GSC-GB pair showed the inverted asymmetric pattern (zone III in Figure 4J) in wild-type H3-expressing testes (Figures 4J and 4K), suggesting that such a pattern is specifically induced by H3T3A-expression.

Expression of H3T3A Causes Several Germline Defects

A spectrum of cellular defects could be detected in *nos>H3T3A* testes after the level of H3T3P is effectively reduced (Figures S2C and S2D). Compared to testes expressing the wild-type H3 (Figures 5A–5D, S4A, S4D, and S5A), H3T3A-expressing testes exhibited phenotypes with both germline and somatic defects (Figures 5E–5H, 5M–5P, S4B, S4E, and S5B). First, GSCs expressing the H3T3A transgene were not maintained properly. In testes without transgene or expressing H3-GFP, only germ cells with dotted spectrosome structure (de Cuevas and Spradling, 1998; Hime et al., 1996; Lin et al., 1994) were detectable next to the hub cells (Figure S4A, arrows). However, in *nos>H3T3A* testes, germ cells with branched fusome structure were detected adjacent to the hub region (arrowheads in Figure S4B), suggesting that GSCs either undergo precocious differentiation or cell death, thereby allowing more differentiated spermatogonial cysts to take their place. Quantification of these two distinct cellular structures (spectrosome versus fusome) showed a significant loss of GSCs in H3T3A-expressing testes (Figure S4C). Second, we observed a significant expansion of germline tumors carrying early-stage cellular markers, including *nos*-driven GFP expression (Figures 5E, 5F, S4E, and S5B), spectrosome structure (Figures 5E, 5G, S4E, S5B, and S5D), and condensed nuclei (Chen et al., 2013; Schulz et al., 2004; Tran et al., 2000) (Figures 5H and S5B). Interestingly, based on these cellular markers, the tumors of progenitor germ cells developed in *nos>H3T3A* testes were noticeably heterogeneous (Figure S5D). For example, some tumor cells maintained strong GFP expression (Figure S5D), a mark indicative of active *nos-Gal4* activity, and exhibited spectrosome structure (Figure S5D), suggesting that they are an early-stage GSC and/or GB cell tumor. Conversely, other tumor cells exhibited loss of GFP expression and a fusome structure (Figure S5D), suggesting that they are a later-stage spermatogonial tumor. We reason that this heterogeneity in tumor types is likely due to the heterogeneity observed in histone inheritance patterns (Figures 3 and 4). Third, the *nos>H3T3A* males had gradually decreased fertility (Figure S5C), consistent with the progression of germline defects (Figure S5B) and eventual germ cell loss (Figures 5M–5P and 5U). While the progenitor germ cell tumor phenotype was not detected in *nos>H3* (n = 19) control testes, it was observed in 42.9% of *nos>H3T3A* testes (n = 42) (Figure 5U). The germ cell loss phenotype was detected in 15.8% of *nos>H3* (n = 19) control testes but in 47.6% of *nos>H3T3A* testes (n = 42) (Figure 5U). The loss of germ cells in 15.8% of control testes is likely due to age-related effect (Boyle et al., 2007; Cheng et al., 2008; Toledano et al., 2012; Wallenfang et al., 2006). Last, *nos>H3T3A* testes (Figures 5G, inset, and S4B, yellow outline) showed a substantial hub enlargement (Figure 5V) compared to *nos>H3* testes (Figures 5C, inset, and S4A, yellow outline), most likely as a secondary defect due to GSC loss as reported previously (Dinardo et al., 2011; Gönczy and DiNardo, 1996; Monk et al., 2010; Tazuke et al., 2002). In summary, development of these germline defects in adult flies suggests that H3T3P is likely required for both GSC maintenance and proper differentiation of GB.

Expression of H3T3A in Late-Stage Germ Cells or Somatic Cells Does Not Cause Germline Tumors

The GSC loss, germline tumor and hub enlargement phenotypes in *nos>H3T3A* testes were specifically caused by expressing H3T3A in early-stage germ cells. We used a later-stage germline driver, *bam-Gal4* (Cheng et al., 2008; Eun et al., 2014; Schulz et al., 2004) (Figure 6A), to turn on the same *H3T3A* transgene in four-cell and later stage germ cells. In doing so, we were able to effectively reduce H3T3P in the more differentiated germ cells (Figure 6G). However, in this population of symmetrically dividing cells, we did not detect the phenotypes (Figures 6J–6M) we had observed in *nos>H3T3A* testes (Figures 5, S4, and S5).

In addition to GSCs, another type of adult stem cell residing in the *Drosophila* testis niche is the cyst stem cell (CySC), which, under normal conditions, is the only mitotically active somatic

(M–T) Immunostaining using a germ cell-specific anti-Vasa in testes from *nos>H3T3A-GFP* (M–P) or *nos>H3T3D-GFP* (Q–T) males. Both germ cell loss (M–T) and germline tumors (white dotted outline in Q–T) are detectable. Hoechst stains nuclei in (D), (H), (L), (P), and (T). Scale bars, 20 μm.

(U) Quantification of the percentage of testes with germline tumor and/or germ cell loss in testes expressing *nos>H3-GFP* (n = 19), *nos>H3T3A-GFP* (n = 42), or *nos>H3T3D-GFP* (n = 43).

(V) Quantification of hub size: 108 ± 2.393 μm^2 in *nos>H3-GFP* (n = 50) testes versus 198.5 ± 15.22 μm^2 in *nos>H3T3A-GFP* testes (n = 37) (***$p < 10^{-4}$) or 145.2 ± 9.702 μm^2 in *nos>H3T3D-GFP* testes (n = 37) (***$p < 10^{-4}$). All ratios = Avg ± SE; p value calculated by unpaired t test.

See also Figures S4 and S5.

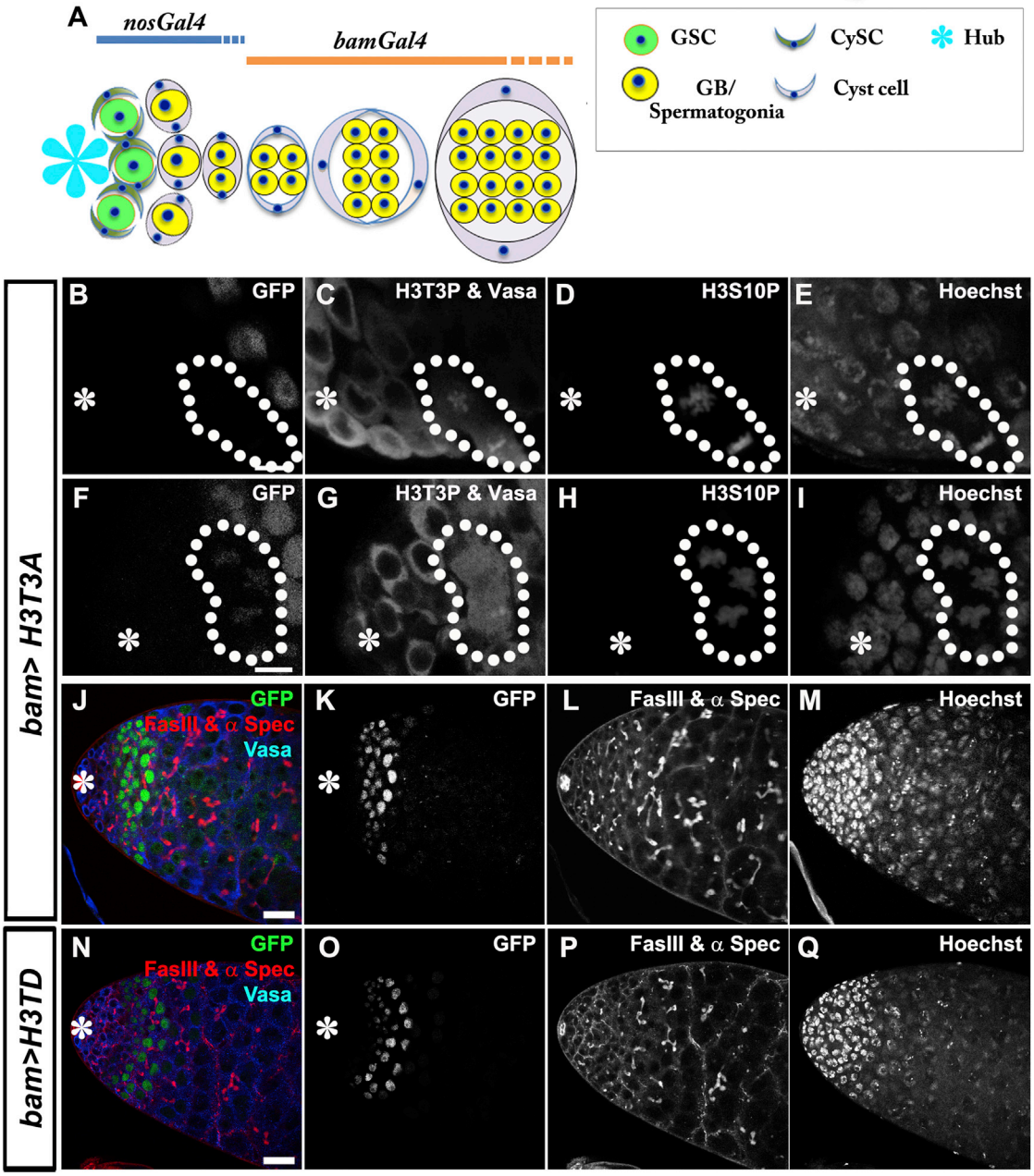

Figure 6. Expression of H3T3A or H3T3D Using the *bam-Gal4* Driver Did Not Phenocopy Defects in *nos>H3T3A* or *nos>H3T3D* Testes

(A) A cartoon showing stage-specificity of *nos-Gal4* and *bam-Gal4* drivers: *nos-Gal4* is turned on in early-stage germline, including GSCs (Van Doren et al., 1998), while *bam-Gal4* expresses from four-cell spermatogonial cells (Cheng et al., 2008; Eun et al., 2014; Schulz et al., 2004).

(B–I) Immunostaining using antibodies against the germ cell-specific marker Vasa, H3T3P, and H3S10P in *bam>H3T3A-GFP* testes. Expression of *bam>H3T3A* greatly reduces H3T3P in later stage mitotic spermatogonial cells: a two-cell mitotic spermatogonial cyst (white dotted outline in B–E) without H3T3A-GFP (B) had detectable H3T3P (C) and H3S10P (D), both H3T3P and H3S10P overlapped with DNA signal stained with Hoechst (E). By contrast, a four-cell mitotic spermatogonial cyst (white dotted outline in F–I) with H3T3A-GFP (F) had greatly reduced H3T3P (G) but abundant H3S10P (H), the H3S10P signal overlapped with DNA signal stained with Hoechst (I). The diffusive signal in (C) and (G) came from anti-Vasa, which stains the entire mitotic germ cells because their nuclear envelopes are broken down (Yadlapalli et al., 2011; Yuan et al., 2012). Scale bars, 10 μm.

(J–Q) Immunostaining using antibodies against a hub marker FasIII, spectrosome/fusome marker α-spectrin and Vasa: tip of the testis expressing *bam>H3T3A-GFP* (J-M) or *bam>H3T3D-GFP* (N-Q). Scale bars, 20 μm. Asterisks in (B–K), (N), and (O), hub.

See also Figure S6.

gonadal cell type (Dinardo et al., 2011). When we used a somatic cell-specific *Tj-Gal4* driver (Tanentzapf et al., 2007) to express H3T3A, we found it is sufficient to reduce H3T3P signal specifically in CySCs (Figure S6A). However, no dramatic cellular defects could be detected when comparing *Tj>H3T3A* (Figure S6C) with *Tj>H3* testes (Figure S6B). In summary, these stage-specific and cell type-specific effects caused by H3T3A expression suggest that the phenotype we observed in *nos>H3T3A* testes is unlikely the result of a global perturbation of general cellular machineries.

Expression of H3T3D in Early-, but Not Late-Stage, Germ Cells Leads to Randomized H3 Inheritance and Cellular Defects

To further understand how H3T3P functions in GSCs, we expressed a different H3T3 mutant for which the T3 residue was converted to the phosphomimetic aspartic acid (D), under the hypothesis that such a mutation may disrupt the temporal order of H3T3 phosphorylation (Figures 1I–1N and S1D). Indeed, expression of H3T3D in early germ cells using a similar dual-color labeling strategy (as described for H3T3A in Figure 3A) also randomizes pre-existing H3T3D and newly synthesized H3T3D inheritance patterns (Figures 4J, 4K, and S3B; Table S1): approximately 79.0% (45/57) of GSC-GB pairs showed symmetric inheritance patterns, 7.0% (4/57) showed conventional asymmetry, and 10.5% (6/57) showed inverted asymmetry, with the remaining 3.5% (2/57) of pairs at the borderline between asymmetry and symmetry (1.45- to 1.55-fold). The randomized H3T3D inheritance patterns cannot be attributed to loss of H3T3P, as H3T3P is still detectable in H3T3D-expressing GSCs (Figure S3C). These data suggest that it is likely the timing of the H3T3 phosphorylation that is important for normal GSC activity.

In addition, both progenitor germline tumor (Figures 5I–5L and S4F) and germ cell loss (Figures 5Q–5T) phenotypes could be detected in *nos-H3T3D* testes (Figure 5U). Quantification showed significant decrease of GSCs in *nos>H3T3D* testes (6.84 ± 0.41, $n = 37$) compared to that of the control *nos>H3* testes (8.68 ± 0.31, $n = 19$; $p < 0.001$). Moreover, similar to the *nos>H3T3A* testes, the hub region in *nos>H3T3D* testes was also enlarged compared to the control *nos>H3* testes (Figures 5V and S4F), most likely as a secondary effect due to the loss of GSCs. By contrast, no germline tumor phenotype was found when the same transgene *H3T3D-GFP* was driven by the *bam-Gal4* driver (Figures 6N–6Q).

Since both reduction of H3T3P by expression of H3T3A and the mimicking of H3T3P by expression of H3T3D result in similar histone inheritance and germline defects, we hypothesize that phosphorylation of H3T3 might require a tight temporal control during GSC mitosis. Therefore, expressing either the H3T3A or the H3T3D may lead to loss of this control and similar defects in histone inheritance patterns as well as abnormal germline activity.

Differential Effects of *haspin* Gene Mutations on Germline Tumor Phenotypes in H3T3A- and H3T3D-Expressing Testes

The kinase that generates the H3T3P mark has been identified to be the Haspin protein (Dai et al., 2005). By driving a short hairpin RNA (shRNA) (Ni et al., 2011) with the *nos-Gal4* driver to knock down *haspin*, specifically in early-stage germ cells, we were able to observe a significant decrease of H3T3P in GSCs (Figure S7A). Testes expressing *nos>haspin shRNA* showed a much greater frequency of cell death (Figures S7C and S7D) confined mainly to spermatogonial cells (Yacobi-Sharon et al., 2013), when compared to the *nos-Gal4* control (Figure S7B). Even though spermatogonial cell death was also detected in *nos>H3T3A* testes (and in *bam>H3T3A* testes), germline tumor phenotype was much more prevalent in *nos>H3T3A* testes than in *nos>haspin shRNA* testes. The similarity between *nos>H3T3A* and *nos>haspin shRNA* phenotypes is consistent with the fact that both lead to reduced H3T3 phosphorylation. The difference between *nos>H3T3A* and *nos>haspin shRNA* phenotypes suggests that the phenotypes induced by H3T3A expression are not simply a byproduct of compromising Haspin kinase activity in general. It is likely that Haspin targets some, as of yet, unknown substrates other than H3T3 in *Drosophila* GSCs. For instance, the yeast Haspin homolog has been shown to have potential roles in regulating mitotic spindle polarity (Panigada et al., 2013). It has also been reported that knockdown of Haspin in human cells (Wang et al., 2010; Yamagishi et al., 2010; reviewed by Higgins, 2010) or in *Xenopus* (Kelly et al., 2010) results in mitotic spindle defects.

To further understand potential interactions between Haspin and loss-of-H3T3P phenotypes, we first asked whether halving the level of Haspin could enhance the *nos>H3T3A* phenotype. For this, we utilized a set of permissive conditions described hereafter to create a sensitized genetic background. Due to the temperature sensitivity of the Gal4:UAS system, flies grown at lower temperature (i.e., 18°C) have been shown to have reduced levels of Gal4-driven expression (Eliazer et al., 2011). In testis samples from *nos>H3T3A* flies grown at 18°C at an earlier developmental stage (3rd instar larvae), we found that H3T3P is still abundant and cellular defects were minimal. For example, no obvious germline tumor was detected ($n = 18$, Figures 7A–7D). Therefore, we utilized these conditions as a permissive but sensitized genetic background. In this background, if Haspin level was halved (using a deficiency chromosome that uncovers the *haspin* gene locus; Figures 7E–7H), increased germ cell tumors could be detected (56%, $n = 19$, Figure 7M). These tumors were identified using a variety of morphological features, including expansion of germ cells with *nos-Gal4*-driving GFP expression (Figure 7F versus 7B), spectrosome structure (Figure 7G versus 7C), and condensed nuclei (Figure 7H versus 7D). Enhancement of the germline tumor phenotype in *nos>H3T3A* testes was also detected using a hypomorphic *haspin^{mi09386}* allele (Venken et al., 2011), although with less severity (Figures 7I–7L) and lower penetrance (21%, $n = 16$, Figure 7M). In summary, these data showed that in *nos>H3T3A* testes the germline tumor phenotype could be enhanced by loss-of-function in *haspin* gene.

We next explored the genetic interaction between *haspin* and *nos>H3T3D* phenotype by utilizing a set of restrictive conditions—flies were grown at 18°C, shifted to 29°C as newly eclosed flies and kept at 29°C for 7 days, under which *nos>H3T3D* testes showed strong phenotype with high penetrance. We found that when Haspin level was halved using the same deficiency chromosome that uncovers the *haspin* gene

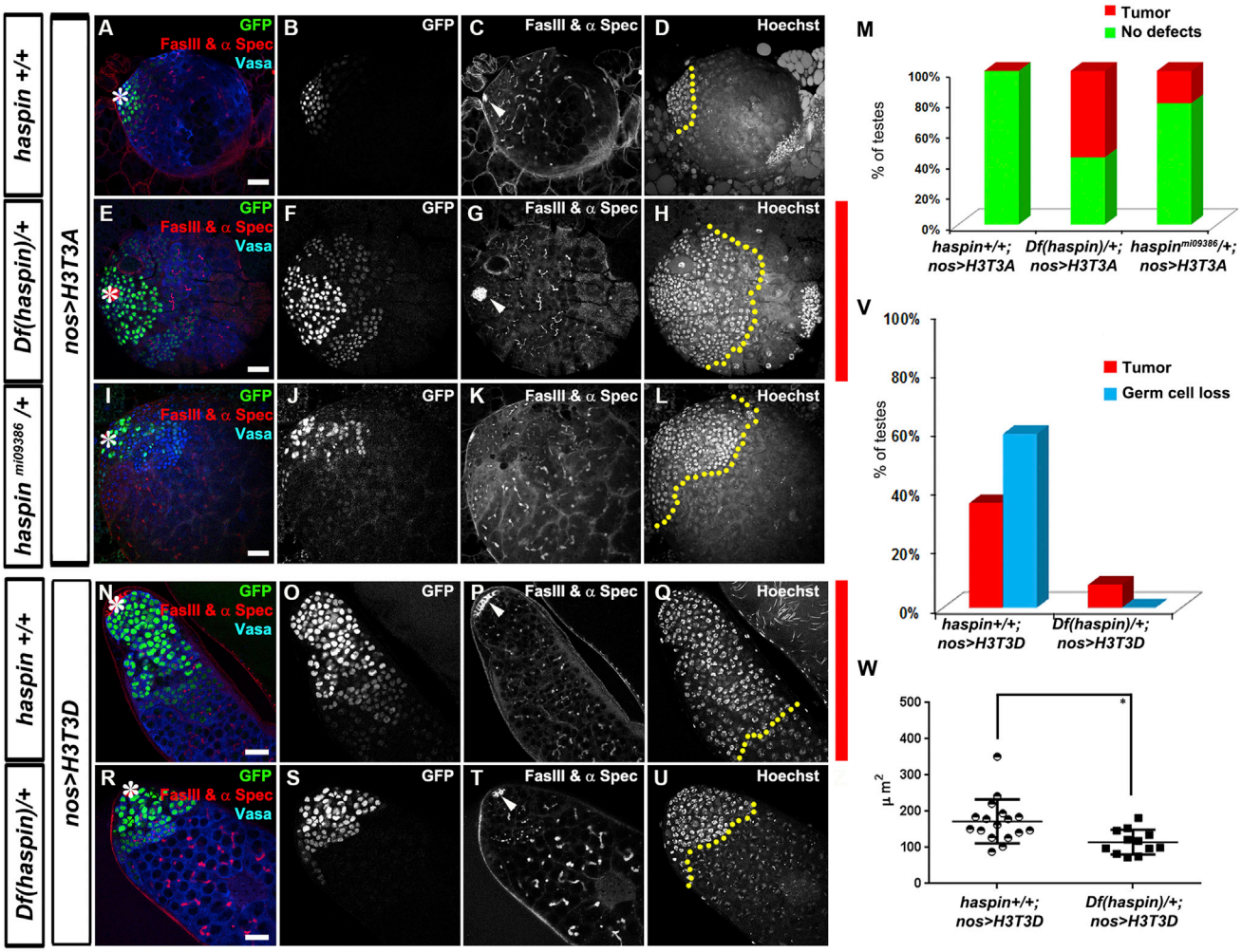

Figure 7. Genetic Interactions between *haspin* Gene Mutants and Mutations of H3T3

(A–L) Immunostaining using antibodies against a hub marker FasIII, spectrosome/fusome marker α-spectrin and germ cell marker Vasa in larval testes from *nos>H3T3A* (A–D), *Df (haspin)/+; nos>H3T3A* (E–H) or *haspin*^{mi09386}*/+; nos>H3T3A* (I–L) males at constant 18°C. Early-stage germline tumor is detected in testes from *Df (haspin)/+; nos>H3T3A* (F) and (H) or *haspin*^{mi09386}*/+; nos>H3T3A* (J) and (L) males, but not in testes from *nos>H3T3A* (B) and (D) males. Arrowhead in (G) points to enlarged hub area compared to (C).

(M) Percentage of testes that are normal or have germline tumor(s) from males of the following genotypes: *nos>H3T3A* (n = 18); *Df (haspin)/+; nos>H3T3A* (n = 16); and *haspin*^{mi09386}*/+; nos>H3T3A* (n = 19).

(N–U) Immunostaining using antibodies against FasIII, α-spectrin, and Vasa in testes from *nos>H3T3D* (N–Q) or *Df (haspin)/+; nos>H3T3D* (R–U) males (siblings from the same crosses) grown at 18°C, shifted to 29°C as newly eclosed flies and kept at 29°C for 7 days. Early-stage germline tumor is detected in testes from *nos>H3T3D* males (O) and (Q), but less severe in testes from *nos>H3T3D; Df (haspin)/+* males (S) and (U). Arrowhead in (P) points to enlarged hub area compared to (T). Early-stage germ cells, as determined by *nos*-driven GFP expression (B), (F), (J), (O), and (S), and nuclear morphology are delineated by the yellow dotted lines in (D), (H), (L), (Q), and (U).

(V) Percentage of testes that have germline tumor(s) or germ cell loss from males with the following genotypes: *nos>H3T3D* (n = 17) or *Df (haspin)/+; nos>H3T3D* (n = 12).

(W) Quantification of hub size: 172.2 ± 14.72 μm^2 in *nos>H3T3D* (n = 17) testes versus 115.0 ± 9.802 μm^2 in *Df (haspin)/+; nos>H3T3D* (n = 12) testes (all ratios = Avg ± SE; *p < 0.005, calculated by unpaired t test). Asterisks in (A), (E), (I), (N), and (R), hub. Scale bars, 20 μm.

See also Figure S7.

locus, both germline tumor and germ cell loss phenotypes in *nos>H3T3D* testes were suppressed, as indicated by lower severity (compare Figures 7N–7Q with Figures 7R–7U) and reduced penetrance (Figure 7V). Consistently, the secondary hub enlargement defect in *nos>H3T3D* testes was also suppressed (Figure 7W). These findings are reminiscent of published studies in which expression of a phosphomimetic substrate can rescue the phenotypes of compromised kinase activity in cancer cells (Wu et al., 2010). Together, the opposite genetic interactions between *haspin* and the two H3 mutations on T3 further support the hypothesis that H3T3P needs to be tightly controlled for proper H3 inheritance and germline activity.

DISCUSSION

Here, we report that a mitosis-enriched H3T3P mark acts as a transient landmark that distinguishes sister chromatids with identical genetic code but different epigenetic information, shown as pre-existing H3-GFP and newly synthesized H3-mKO. By distinguishing sister chromatids containing different epigenetic information, H3T3P functions to allow these molecularly distinct sisters to be segregated and inherited differentially to the two daughter cells derived from one asymmetric cell division. The selective segregation of different populations of histones likely allows these two cells to assume distinct fates: self-renewal versus differentiation. Consequently, loss of proper epigenetic inheritance might lead to defects in both GSC maintenance and GB differentiation, suggesting that both cells need this active partitioning process to either "remember" or "reset" their molecular properties.

The temporal and spatial specificities of H3T3P make it a great candidate to regulate asymmetric sister chromatid segregation. First, H3T3P is only detectable from prophase to metaphase, the window of time during which the mitotic spindle actively tries to attach to chromatids through microtubule-kinetochore interactions. Second, the H3T3P signal is enriched at the peri-centromeric region, where kinetochore components robustly crosstalk with chromatin-associate factors. Third, H3T3 shows a sequential order of phosphorylation, first appearing primarily on sister chromatids enriched with pre-existing H3 and then subsequently appearing on sister chromatids enriched with newly synthesized H3 as the GSC nears metaphase. The distinct temporal patterns shown by H3T3P are unique to GSCs and would allow the mitotic machinery to differentially recognize sister chromatids bearing distinct epigenetic information; an essential step necessary for proper segregation during asymmetric GSC division. Furthermore, the tight temporal control of H3T3 phosphorylation suggests that rather than serving as an inherited epigenetic signature, H3T3P may act as transient signaling mark to allow for the proper partitioning of H3. We hypothesize that H3T3P needs to be under tight temporal control in order to ensure proper H3 inheritance and germline activity.

Our studies have shown that H3T3P is indeed subject to stringent temporal controls during mitosis. The H3T3P mark is undetectable during G2 phase. Upon entry to mitosis, sister chromatids enriched with pre-existing H3-GFP histone begin to show H3T3 phosphorylation prior to sister chromatids enriched with newly synthesized H3-mKO. As the cell continues to progress toward metaphase, H3T3P signal begins to appear on sister chromatids enriched with newly synthesized H3-mKO. Such a tight regulation of H3T3P is compromised when levels of H3T3P are altered due to the incorporation of mutant H3T3A or H3T3D. Incorporation of the H3T3A mutant results in a significant decrease in the levels of H3T3P on sister chromatids throughout mitosis, such that neither sister becomes enriched with H3T3P as the GSC progresses toward metaphase. Conversely, incorporation of the H3T3D mutant would result in seemingly elevated levels of H3T3P early in mitosis. Although H3T3A and H3T3D act in different ways, both mutations significantly disrupt the highly regulated temporal patterns associated with H3T3 phosphorylation, the result of which is randomized H3 inheritance patterns and germ cell defects in testes expressing either H3T3A or H3T3D.

To further evaluate the extent of H3T3A and H3T3D roles in the segregation of sister chromatids enriched with different populations of H3 during mitosis (Figure 1B, step two), we modeled all possible segregation patterns in male GSCs and compared these estimates to our experimental results. To simplify our calculations, we made two important assumptions: first, we assume nucleosomal density to be even throughout the genome. This assumption allows us to infer that the overall fluorescent signal contributed by each chromosome is proportional to their respective number of DNA base pairs. Second, by quantifying pre-existing H3-GFP asymmetry in anaphase and telophase GSCs, we estimate that the establishment of H3-GFP asymmetry is ~4-fold biased, i.e., 80% on one set of sister chromatids and 20% on the other set of sister chromatids, based on quantification of GFP signal in anaphase (GFP GSC side/GB side = 4.5) and telophase (GFP GSC side/GB side = 3.8) GSCs (Tran et al., 2012). With these two simplifying assumptions, we calculate both GFP and mKO ratios among all 64 possible combinations (Table S2: 2 (for X-ch) × 2 (for Y-ch) × 4 (for 2nd ch) × 4 (for 3rd ch) = 64 combinations in total). If we define asymmetry as a greater than ~1.5-fold difference in fluorescence intensity, then based on a model of randomized sister chromatid segregation, we estimate that a symmetric pattern should appear for 53.1% (34/64) of GSC-GB pairs whereas both conventional and inverted asymmetric patterns should occur with equal frequencies and account for 18.7% (12/64) of total GSC-GB pairs. The remaining 9.4% (6/64) of GSC-GB pairs should produce histone inheritance patterns with a 1.45- to 1.55-fold difference in signal intensity (predicted ratios in Figure 4K).

This estimation is close to our experimental data in both H3T3A- and H3T3D-expressing testes (Figures 4J and 4K; Table S1). Of the 64 quantified post-mitotic GSC-GB pairs in *nos>H3T3A* testes, ~71.9% showed symmetric inheritance pattern. Conventional and inverted asymmetric patterns were detected at 9.4% and 12.5%, respectively, and 6.3% at the borderline. Similarly, of the 57 quantified post-mitotic GSC-GB pairs in *nos>H3T3D* testes, ~79.0% showed symmetric inheritance pattern. Conventional and inverted asymmetric patterns were detected at 7.0% and 10.5%, respectively with 3.5% of pairs at the borderline. Some differences between predicted ratios and our experimental data could be due to the simplified assumptions, the limited sensitivity of our measurement, and/or some coordinated chromatid segregation modes that bias the eventual read-out (Yadlapalli and Yamashita, 2013). In summary, comparison between the modeling ratios and our experimental data suggest that loss of the tight control of H3T3 phosphorylation in GSCs randomizes segregation of sister chromatids enriched with different populations of H3.

If the temporal separation in the phosphorylation of H3T3 on epigenetically distinct sister chromatids facilitates their proper segregation and inheritance during asymmetric cell division, it is likely that mutations of the Haspin kinase will also affect the temporal control of H3T3 phosphorylation. In the context of H3T3A, where the levels of H3T3P are already reduced, a further decrease in H3T3P by reducing Haspin levels should limit the GSC's ability to distinguish between sister chromatids enriched

with distinct H3. Indeed, *haspin* mutants enhance the phenotypes in *nos>H3T3A* testes. A different situation appears in the context of H3T3D where sister chromatids experience seemingly elevated levels of H3T3P at the start of mitosis. These elevated H3T3P levels may be exacerbated by the phosphorylation activity of the Haspin kinase. Therefore, it is conceivable that by halving the levels of the Haspin kinase, H3T3 phosphorylation should be reduced to a level more closely resembling wild-type. In this way, some of the temporal specificity that is lost in the H3T3D mutant is restored, resulting in suppression of the phenotypes observed in *nos>H3T3D* testes. An exciting topic for future study would be to further explore how exactly Haspin phosphorylates H3T3 in the context of chromatin and whether H3T3A and H3T3D mutations act synergistically or antagonistically in regulating asymmetric sister chromatids segregation through differential phosphorylation of a key histone residue.

It would also be interesting to understand the potential connection between asymmetric histone inheritance and another phenomenon reported by several investigators: selective DNA strand segregation (reviewed by Evano and Tajbakhsh, 2013; Rando, 2007; Tajbakhsh and Gonzalez, 2009). Recent development of the chromosome orientation fluorescence in situ hybridization (CO-FISH) technique (Falconer et al., 2010) allows study of selective chromatid segregation at single-chromosome resolution. Using this technique in mouse satellite cells, it has been demonstrated that all chromosomes are segregated in a biased manner, such that pre-existing template DNA strands are preferentially retained in the daughter cell that retains stem cell identity. Interestingly, this biased segregation becomes randomized in progenitor non-stem cells (Rocheteau et al., 2012). Using CO-FISH in *Drosophila* male GSCs, sex chromosomes have been shown to segregate in a biased manner. Remarkably, sister chromatids from homologous autosomes have been shown to co-segregate independent of any specific strand preference (Yadlapalli and Yamashita, 2013). Such findings hint at a possible epigenetic source guiding the coordinated inheritance of *Drosophila* homologous autosomes. In many cases of biased inheritance, researchers have speculated about the existence of a molecular signature that would allow the cell to recognize and segregate sister chromatids bearing differential epigenetic information (Klar, 1994, 2007; Lansdorp, 2007; Rando, 2007; Yennek and Tajbakhsh, 2013). However, the identity of such a signature has remained elusive. The work represented in this paper provides experimental evidence demonstrating that a tightly-controlled histone modification, H3T3P, is able to distinguish sister chromatids and coordinate their segregation.

Epigenetic processes play important roles in regulating stem cell identity and activity. Failure to appropriately regulate epigenetic information may lead to abnormalities in stem cell behaviors, which underlie early progress toward diseases such as cancer and tissue degeneration. Due to the crucial role that such processes play in regulating cell identity and behavior, the field has long sought to understand whether and how stem cells maintain their epigenetic memory through many cell divisions. Our results here suggest that the asymmetric segregation of pre-existing and newly synthesized H3-enriched chromosomes may function to determine distinct cell fates of GSCs versus differentiating daughter cells.

EXPERIMENTAL PROCEDURES

Heat-Shock Scheme

Flies with *UASp-FRT-H3-GFP-PolyA-FRT-H3- mKO* or *UASp-FRT-H3T3A/D-GFP-PolyA-FRT-H3T3A/D- mKO* mutant transgene were paired with *nos-Gal4* drivers. Flies were raised at 18°C throughout development until adulthood to avoid pre-flip (Tran et al., 2012). Before heat shock, 0- to 3-day-old males were transferred to vials that had been air-dried for 24 hr. Vials were submerged underneath water up to the plug in a circulating 37°C water bath for 2 hr and recovered in a 29°C incubator for indicated time before dissection and immunostaining experiments.

Temperature Shift Assay to Induce Germline Tumor in Adult Flies

Flies with *UASp-FRT-H3-GFP-PolyA-FRT-H3- mKO* or *UASp-FRT-H3T3A/D-GFP-PolyA-FRT-H3T3A/D- mKO* paired with *nos-Gal4*, *bam-Gal4*, or *Tj-Gal4* driver were raised at 18°C throughout development until adulthood. Newly enclosed males were collected and shifted to 29°C for indicated time before dissection and immunostaining experiments.

Immunostaining Experiments

Immunofluorescence staining was performed using standard procedures (Hime et al., 1996; Tran et al., 2012). Primary antibodies were mouse anti-α spectrin (1:50, DSHB 3A9), mouse anti-Fas III (1:50, DSHB, 7G10), mouse anti-Armadillo (1:100; DSHB, N2 7A1 clone), rabbit anti- H3T3P (1:200, Millipore 05-746R), mouse anti-H3S10P (1:2,000; Millipore, #05-806), chicken anti-CID (1:100; gift from Dr. Sylvia Erhardt, University of Heidelberg, Germany), and rabbit anti-Vasa (1:200; Santa Cruz SC-30210). Secondary antibodies were the Alexa Fluor-conjugated series (1:200; Molecular Probes). Lysotracker (Invitrogen L7528) is applied according to manufacturer recommendation. Images were taken using the Zeiss LSM 510 META or Zeiss LSM 700 Multiphoton confocal microscope with a 40× or 63× oil immersion objectives and processed using Adobe Photoshop software.

EdU Incorporation to Label GSC-GB Pair at S Phase

EdU labeling of the GSC-GB pairs at S phase was performed using Click-iT EdU Alexa Fluor 647 Imaging Kit (Life Science C10640) according to manufacturer's instructions. Dissected testes were immediately incubated in S2 medium with 100 μM EdU for 30 min at room temperature. The testes were subsequently fixed and proceed to primary antibodies (anti-FasIII, anti-α spectrin and anti-Vasa) incubation. Fluorophore conjugation to EdU was performed along manufacturer's instructions and followed by secondary antibodies incubation.

The addition of EdU facilitates recognition of the GSC-GB pairs undergoing active DNA synthesis from those without EdU, which might be arrested due to the heat-shock treatment. The cell-cycle progression is important for the incorporation and segregation of pre-existing versus newly synthesized H3.

Quantification of GFP and mKO Intensity

No antibody was added to enhance either GFP or mKO signal. Values of GFP and mKO intensity were calculated using Image J software. DAPI signal was used to determine the area of nucleus for measuring both GFP and mKO fluorescent signals, the raw reading was subsequently adjusted by subtracting fluorescence signals in the hub region used as background in both GSC and GB nuclei and compared between each other.

SUPPLEMENTAL INFORMATION

Supplemental Information includes Supplemental Experimental Procedures, seven figures, and two tables and can be found with this article online at http://dx.doi.org/10.1016/j.cell.2015.10.002.

AUTHOR CONTRIBUTIONS

Conceptualization, J.X. and X.C.; Methodology, J.X., V.T., B.-C.C., M.W., E.B., and X.C.; Investigation, J.X., V.T., B.-C.C., M.W., C.P., and C.S.; Writing – Original Draft, J.X., M.W., and X.C.; Funding Acquisition, E.B. and X.C.; Supervision, E.B. and X.C.

ACKNOWLEDGMENTS

We thank S. Erhardt for anti-CID and Y-S. Lee, A. Spradling, M. Van Doren, R. Johnston, E. Moudrianakis, A. Hoyt, Y. Yamashita, K. Zhao, and X.C. lab members for suggestions. We thank Johns Hopkins Integrated Imaging Center for confocal imaging. Supported by NIH R01HD065816 and R01GM112008, the David and Lucile Packard Foundation, Johns Hopkins University start-up (X.C.), NIH 5T32GM007231 (M.W.), and Howard Hughes Medical Institute (E.B. and B.-C.C.).

Received: May 22, 2015
Revised: August 8, 2015
Accepted: September 22, 2015
Published: October 29, 2015

REFERENCES

Betschinger, J., and Knoblich, J.A. (2004). Dare to be different: asymmetric cell division in Drosophila, C. elegans and vertebrates. Curr. Biol. *14*, R674–R685.

Bonasio, R., Tu, S., and Reinberg, D. (2010). Molecular signals of epigenetic states. Science *330*, 612–616.

Boyle, M., Wong, C., Rocha, M., and Jones, D.L. (2007). Decline in self-renewal factors contributes to aging of the stem cell niche in the Drosophila testis. Cell Stem Cell *1*, 470–478.

Caperta, A.D., Rosa, M., Delgado, M., Karimi, R., Demidov, D., Viegas, W., and Houben, A. (2008). Distribution patterns of phosphorylated Thr 3 and Thr 32 of histone H3 in plant mitosis and meiosis. Cytogenet. Genome Res. *122*, 73–79.

Chen, H., Chen, X., and Zheng, Y. (2013). The nuclear lamina regulates germline stem cell niche organization via modulation of EGFR signaling. Cell Stem Cell *13*, 73–86.

Cheng, J., Türkel, N., Hemati, N., Fuller, M.T., Hunt, A.J., and Yamashita, Y.M. (2008). Centrosome misorientation reduces stem cell division during ageing. Nature *456*, 599–604.

Clevers, H. (2005). Stem cells, asymmetric division and cancer. Nat. Genet. *37*, 1027–1028.

Dai, J., Sultan, S., Taylor, S.S., and Higgins, J.M. (2005). The kinase haspin is required for mitotic histone H3 Thr 3 phosphorylation and normal metaphase chromosome alignment. Genes Dev. *19*, 472–488.

de Cuevas, M., and Spradling, A.C. (1998). Morphogenesis of the Drosophila fusome and its implications for oocyte specification. Development *125*, 2781–2789.

Deal, R.B., Henikoff, J.G., and Henikoff, S. (2010). Genome-wide kinetics of nucleosome turnover determined by metabolic labeling of histones. Science *328*, 1161–1164.

Dinardo, S., Okegbe, T., Wingert, L., Freilich, S., and Terry, N. (2011). lines and bowl affect the specification of cyst stem cells and niche cells in the Drosophila testis. Development *138*, 1687–1696.

Dion, M.F., Kaplan, T., Kim, M., Buratowski, S., Friedman, N., and Rando, O.J. (2007). Dynamics of replication-independent histone turnover in budding yeast. Science *315*, 1405–1408.

Eliazer, S., Shalaby, N.A., and Buszczak, M. (2011). Loss of lysine-specific demethylase 1 nonautonomously causes stem cell tumors in the Drosophila ovary. Proc. Natl. Acad. Sci. USA *108*, 7064–7069.

Escribá, M.C., and Goday, C. (2013). Histone H3 phosphorylation and elimination of paternal X chromosomes at early cleavages in sciarid flies. J. Cell Sci. *126*, 3214–3222.

Eun, S.H., Shi, Z., Cui, K., Zhao, K., and Chen, X. (2014). A non-cell autonomous role of E(z) to prevent germ cells from turning on a somatic cell marker. Science *343*, 1513–1516.

Evano, B., and Tajbakhsh, S. (2013). Sorting DNA with asymmetry: a new player in gene regulation? Chromosome Res. *21*, 225–242.

Falconer, E., Chavez, E.A., Henderson, A., Poon, S.S., McKinney, S., Brown, L., Huntsman, D.G., and Lansdorp, P.M. (2010). Identification of sister chromatids by DNA template strand sequences. Nature *463*, 93–97.

Gönczy, P., and DiNardo, S. (1996). The germ line regulates somatic cyst cell proliferation and fate during Drosophila spermatogenesis. Development *122*, 2437–2447.

Herz, H.M., Morgan, M., Gao, X., Jackson, J., Rickels, R., Swanson, S.K., Florens, L., Washburn, M.P., Eissenberg, J.C., and Shilatifard, A. (2014). Histone H3 lysine-to-methionine mutants as a paradigm to study chromatin signaling. Science *345*, 1065–1070.

Higgins, J.M. (2010). Haspin: a newly discovered regulator of mitotic chromosome behavior. Chromosoma *119*, 137–147.

Hime, G.R., Brill, J.A., and Fuller, M.T. (1996). Assembly of ring canals in the male germ line from structural components of the contractile ring. J. Cell Sci. *109*, 2779–2788.

Inaba, M., and Yamashita, Y.M. (2012). Asymmetric stem cell division: precision for robustness. Cell Stem Cell *11*, 461–469.

Kelly, A.E., Ghenoiu, C., Xue, J.Z., Zierhut, C., Kimura, H., and Funabiki, H. (2010). Survivin reads phosphorylated histone H3 threonine 3 to activate the mitotic kinase Aurora B. Science *330*, 235–239.

Klar, A.J. (1994). A model for specification of the left-right axis in vertebrates. Trends Genet. *10*, 392–396.

Klar, A.J. (2007). Lessons learned from studies of fission yeast mating-type switching and silencing. Annu. Rev. Genet. *41*, 213–236.

Lansdorp, P.M. (2007). Immortal strands? Give me a break. Cell *129*, 1244–1247.

Lewis, P.W., Müller, M.M., Koletsky, M.S., Cordero, F., Lin, S., Banaszynski, L.A., Garcia, B.A., Muir, T.W., Becher, O.J., and Allis, C.D. (2013). Inhibition of PRC2 activity by a gain-of-function H3 mutation found in pediatric glioblastoma. Science *340*, 857–861.

Lin, H., Yue, L., and Spradling, A.C. (1994). The Drosophila fusome, a germline-specific organelle, contains membrane skeletal proteins and functions in cyst formation. Development *120*, 947–956.

Markaki, Y., Christogianni, A., Politou, A.S., and Georgatos, S.D. (2009). Phosphorylation of histone H3 at Thr3 is part of a combinatorial pattern that marks and configures mitotic chromatin. J. Cell Sci. *122*, 2809–2819.

Martin, C., and Zhang, Y. (2007). Mechanisms of epigenetic inheritance. Curr. Opin. Cell Biol. *19*, 266–272.

Monk, A.C., Siddall, N.A., Volk, T., Fraser, B., Quinn, L.M., McLaughlin, E.A., and Hime, G.R. (2010). HOW is required for stem cell maintenance in the Drosophila testis and for the onset of transit-amplifying divisions. Cell Stem Cell *6*, 348–360.

Morrison, S.J., and Kimble, J. (2006). Asymmetric and symmetric stem-cell divisions in development and cancer. Nature *441*, 1068–1074.

Ni, J.Q., Zhou, R., Czech, B., Liu, L.P., Holderbaum, L., Yang-Zhou, D., Shim, H.S., Tao, R., Handler, D., Karpowicz, P., et al. (2011). A genome-scale shRNA resource for transgenic RNAi in Drosophila. Nat. Methods *8*, 405–407.

Panigada, D., Grianti, P., Nespoli, A., Rotondo, G., Castro, D.G., Quadri, R., Piatti, S., Plevani, P., and Muzi-Falconi, M. (2013). Yeast haspin kinase regulates polarity cues necessary for mitotic spindle positioning and is required to tolerate mitotic arrest. Dev. Cell *26*, 483–495.

Polioudaki, H., Markaki, Y., Kourmouli, N., Dialynas, G., Theodoropoulos, P.A., Singh, P.B., and Georgatos, S.D. (2004). Mitotic phosphorylation of histone H3 at threonine 3. FEBS Lett. *560*, 39–44.

Rando, T.A. (2007). The immortal strand hypothesis: segregation and reconstruction. Cell *129*, 1239–1243.

Rocheteau, P., Gayraud-Morel, B., Siegl-Cachedenier, I., Blasco, M.A., and Tajbakhsh, S. (2012). A subpopulation of adult skeletal muscle stem cells retains all template DNA strands after cell division. Cell *148*, 112–125.

Schulz, C., Kiger, A.A., Tazuke, S.I., Yamashita, Y.M., Pantalena-Filho, L.C., Jones, D.L., Wood, C.G., and Fuller, M.T. (2004). A misexpression screen reveals effects of bag-of-marbles and TGF beta class signaling on the Drosophila male germ-line stem cell lineage. Genetics *167*, 707–723.

Sheng, X.R., and Matunis, E. (2011). Live imaging of the Drosophila spermatogonial stem cell niche reveals novel mechanisms regulating germline stem cell output. Development *138*, 3367–3376.

Tajbakhsh, S., and Gonzalez, C. (2009). Biased segregation of DNA and centrosomes: moving together or drifting apart? Nat. Rev. Mol. Cell Biol. *10*, 804–810.

Tanentzapf, G., Devenport, D., Godt, D., and Brown, N.H. (2007). Integrin-dependent anchoring of a stem-cell niche. Nat. Cell Biol. *9*, 1413–1418.

Tazuke, S.I., Schulz, C., Gilboa, L., Fogarty, M., Mahowald, A.P., Guichet, A., Ephrussi, A., Wood, C.G., Lehmann, R., and Fuller, M.T. (2002). A germline-specific gap junction protein required for survival of differentiating early germ cells. Development *129*, 2529–2539.

Toledano, H., D'Alterio, C., Czech, B., Levine, E., and Jones, D.L. (2012). The let-7-Imp axis regulates ageing of the Drosophila testis stem-cell niche. Nature *485*, 605–610.

Tran, J., Brenner, T.J., and DiNardo, S. (2000). Somatic control over the germline stem cell lineage during Drosophila spermatogenesis. Nature *407*, 754–757.

Tran, V., Lim, C., Xie, J., and Chen, X. (2012). Asymmetric division of Drosophila male germline stem cell shows asymmetric histone distribution. Science *338*, 679–682.

Tran, V., Feng, L., and Chen, X. (2013). Asymmetric distribution of histones during Drosophila male germline stem cell asymmetric divisions. Chromosome Res. *21*, 255–269.

Van Doren, M., Williamson, A.L., and Lehmann, R. (1998). Regulation of zygotic gene expression in Drosophila primordial germ cells. Curr. Biol. *8*, 243–246.

Venken, K.J., Schulze, K.L., Haelterman, N.A., Pan, H., He, Y., Evans-Holm, M., Carlson, J.W., Levis, R.W., Spradling, A.C., Hoskins, R.A., and Bellen, H.J. (2011). MiMIC: a highly versatile transposon insertion resource for engineering Drosophila melanogaster genes. Nat. Methods *8*, 737–743.

Wallenfang, M.R., Nayak, R., and DiNardo, S. (2006). Dynamics of the male germline stem cell population during aging of Drosophila melanogaster. Aging Cell *5*, 297–304.

Wang, F., Dai, J., Daum, J.R., Niedzialkowska, E., Banerjee, B., Stukenberg, P.T., Gorbsky, G.J., and Higgins, J.M. (2010). Histone H3 Thr-3 phosphorylation by Haspin positions Aurora B at centromeres in mitosis. Science *330*, 231–235.

Wu, Q., Sahasrabudhe, R.M., Luo, L.Z., Lewis, D.W., Gollin, S.M., and Saunders, W.S. (2010). Deficiency in myosin light-chain phosphorylation causes cytokinesis failure and multipolarity in cancer cells. Oncogene *29*, 4183–4193.

Yacobi-Sharon, K., Namdar, Y., and Arama, E. (2013). Alternative germ cell death pathway in Drosophila involves HtrA2/Omi, lysosomes, and a caspase-9 counterpart. Dev. Cell *25*, 29–42.

Yadlapalli, S., and Yamashita, Y.M. (2013). Chromosome-specific nonrandom sister chromatid segregation during stem-cell division. Nature *498*, 251–254.

Yadlapalli, S., Cheng, J., and Yamashita, Y.M. (2011). Drosophila male germline stem cells do not asymmetrically segregate chromosome strands. J. Cell Sci. *124*, 933–939.

Yamagishi, Y., Honda, T., Tanno, Y., and Watanabe, Y. (2010). Two histone marks establish the inner centromere and chromosome bi-orientation. Science *330*, 239–243.

Yennek, S., and Tajbakhsh, S. (2013). DNA asymmetry and cell fate regulation in stem cells. Semin. Cell Dev. Biol. *24*, 627–642.

Yuan, H., Chiang, C.Y., Cheng, J., Salzmann, V., and Yamashita, Y.M. (2012). Regulation of cyclin A localization downstream of Par-1 function is critical for the centrosome orientation checkpoint in Drosophila male germline stem cells. Dev. Biol. *361*, 57–67.